

Valence and Spin fluctuations in Mn-doped ferroelectric BaTiO₃

Subhasish Mandal,^{1,2} R. E. Cohen,^{2,3} and K. Haule⁴

¹*Department of Applied Physics, Yale University, New Haven, Connecticut 06511, USA*

²*Extreme Materials Initiative, Geophysical Laboratory,*

Carnegie Institution for Science, Washington D.C. 20015, USA

³*Department of Earth and Environmental Sciences, LMU Munich, 80333 Munich, Germany*

⁴*Department of Physics, Rutgers University, Piscataway, New Jersey 08854, USA*

We study Mn substitution for Ti in BaTiO₃ with and without compensating oxygen vacancies using density functional theory (DFT) in combination with dynamical mean field theory (DMFT). We find strong charge and spin fluctuations. Without compensating oxygen vacancies, the ground state is found to be a quantum superposition of two distinct atomic valences, $3d^4$ and $3d^5$. Introducing a compensating oxygen vacancy at a neighboring site reduces both charge and spin fluctuations due to the reduction of electron hopping from Mn to its ligands. As a consequence, valence fluctuations are reduced, and the valence is closely fixed to the high spin $3d^5$ state. Here we show that inclusion of charge and spin fluctuations is necessary to obtain an accurate ground state of transition metal doped ferroelectrics.

PACS numbers: 74.70.Xa, 74.25.Jb, 75.10.Lp

I. INTRODUCTION

Multiferroics respond to both electric and magnetic fields, and their coupling is an exciting field of research for both understanding their fundamental physics and for potential device applications. One promising route to magnetoelectric materials is to dope ferroelectrics with magnetic ions^{1–4}. Such materials are of interest for electronics that can integrate data processing and memory operation in a single solid state device^{1,2,5,6}. Many commercial transducer materials are doped with transition metal impurities to improve piezoelectric properties, mechanical quality factor, and coercive field, and to decrease electrical conductivity^{1–3,5–15}, but the exact role of the doped impurities is unclear. Defect dipoles formed by transition metal dopants with oxygen vacancy neighbors can greatly enhance electromechanical coupling^{16–20}. Thus, the electronic structure of transition metal dopants is of great interest in general, and in particular in multiferroics and dilute magnetic semiconductors^{21,22}.

When a transition metal ion is doped into a classic ferroelectric material like BaTiO₃, whether the impurity would be an acceptor or a donor of electrons depends on the number of valence electrons and $3d$ occupation, i.e. oxidation state. Valence, charge, or oxidation state are concepts commonly used in chemistry. Oxidation state is an ill-defined quantity in quantum mechanics, although it has proven extremely useful in chemical intuition^{23–29}. Oxidation state can be a point of confusion as very often the charge or oxidation state of a cation differs significantly from the Born transverse effective charges, or the static charges computed by projection onto local or Wannier orbitals or from orbital occupations^{24–28}. The d -occupation remains invariant in charge order driven metal-insulator transitions²⁴, but does depend on the choice of orbitals. The d occupation is also related to the ion magnetic moment.

Mn commonly has three different oxidation states

(Mn⁴⁺, Mn³⁺, Mn²⁺) in perovskites. Mn⁴⁺ and Mn²⁺ have an electronic configuration of d^5 and d^5 respectively, or half-filled t_{2g} or $t_{2g}+e_g$ manifolds in octahedral symmetry. Which states of valence the paramagnetic ions are incorporated into the BaTiO₃ and other perovskites is an open and long standing problem^{7–15,30}. The magnetic moment of Mn substituting for Ti on the B-site in Mn doped BTO without any compensating oxygen vacancy is $3 \mu_B$ (Mn⁴⁺)^{18,31} in conventional DFT and DFT+U. Electron paramagnetic resonance (EPR) and X-ray photoelectron spectroscopic measurements on Mn doped BTO show that Mn can exist in various charge states in BTO; some EPR measurements performed on Mn doped BTO nanoparticle show a high spin state of Mn with the moment of $5 \mu_B$ (Mn²⁺)⁶, whereas Mn⁴⁺ with $3\mu_B$ is also found⁷. The oxidation state of the Mn depends on the oxygen fugacity during growth or annealing, and depends on the concentration of compensating oxygen vacancies or other impurities and defects. Using density functional calculations, Nossa *et al.* found that depending on the oxygen vacancy, Mn ions in BaTiO₃ can exist either on high spin state (Mn²⁺) or low spin state (Mn⁴⁺)¹⁸.

In this paper, we carefully investigate electronic structure of Mn doped BTO with and without compensating O-vacancies in the paramagnetic phase of Mn. Using a *state-of-the-art* DFT+DMFT method, we focus on understanding the charge and spin states Mn exhibits in these prototypical systems in order to combine both d^0 states and partially occupied d -states to unite ferroelectricity and magnetism in one material. We compare our results with conventional DFT and DFT+U in the ferromagnetic phase of Mn. We then describe the effects of oxygen vacancies on the charge and spin fluctuations of Mn and explore the change in local magnetic moment of Mn.

II. METHODS AND STRUCTURAL DETAILS

To understand better the electronic structure of transition metal dopants in dielectrics, in general, and $\text{Mn}_{\text{Ti}}\pm\text{V}_\text{O}$ in BaTiO_3 in particular, we use dynamical mean-field theory (DMFT)³², a sophisticated method, which includes quantum dynamical effects, and takes into account both valence and spin fluctuations. In contrast, DFT includes only average interactions, and DFT+U includes only a single configuration, ignoring multiplet effects. DFT+DMFT has been very successful in describing strongly correlated materials like high temperature superconductors, Mott insulators and several transition metal bearing compounds^{33–42}. In DFT+DMFT, the self-energy that samples all local skeleton Feynman diagrams is added to the DFT Kohn-Sham Hamiltonian^{32,43}. This implementation is fully self-consistent^{35,43}. The iterations stop after full convergence of the charge density, the impurity level, the chemical potential, the self-energy, and the lattice and impurity Green's functions. The lattice is represented using the full potential linear augmented plane wave (LAPW) method, implemented in the Wien2k⁴⁴ package in its generalized gradient approximation (Wu-Cohen-GGA)⁴⁵. The continuous time quantum Monte Carlo method is used to solve the quantum impurity problem and to obtain the local self-energy due to the correlated Mn 3d orbitals. The self-energy is analytically continued from the imaginary to real axis using an auxiliary Green's function to obtain the partial density of states. A fine k-point mesh of at least $4 \times 4 \times 4$ k-points in Monkhorst-Pack k-point grid and a total 40 million Monte Carlo steps for each iteration are used for the paramagnetic phase of the Mn doped BTO at $T=300\text{K}$. The Coulomb interaction U and Hund's coupling J_H are fixed at 6.0 eV and 0.8 eV, respectively⁴⁶, and we have tested varying these parameters. We use the fully localized limit (FLL) double counting⁴⁷, as well as “exact” double counting⁴⁸. For DFT and DFT+U, we use the all electron LAPW method as implemented in WIEN2k⁴⁴. The same U and J_H of 6.0 eV and 0.8 eV are used for DFT+U computations respectively.

We study a paramagnetic Mn dopant in a supercell with $(\text{Mn}_{\text{Ti}}\text{V}_\text{O})$ and without (Mn_{Ti}) a neighboring compensating oxygen vacancy using DFT-DMFT⁴⁹ computation at room temperature. Two $2 \times 2 \times 2$ supercell structures are considered here; one structure with one Mn-replacing Ti atom, and the other structure is with Mn-replacing Ti with an Oxygen vacancy along c-axis. These structures were optimized using DFT+U as implemented in ABINIT^{50,51} and also used in Ref.¹⁸ to understand the role of Mn doping in BTO. For DFT computations, we consider ferromagnetic order with a single Mn-atom in the supercell.

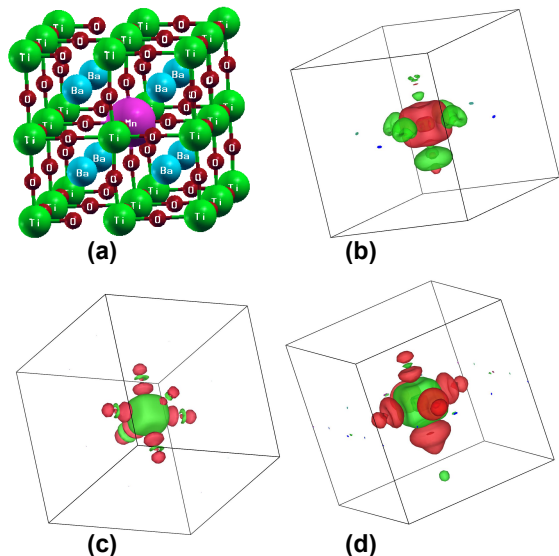


FIG. 1. (Color online) (a) Schematic representation of the structure for Mn-doped (at Ti-site) BaTiO_3 without any compensating oxygen vacancy. Isosurface plot of electron density difference between (b) DFT and DFT+U (c) DFT and DFT+DMFT and (d) DFT+U and DFT+DMFT methods. The green or red means increase or decrease of $0.85 \times 10^{-3} \text{ e} / \text{\AA}^3$ upon the DMFT calculation.

III. RESULTS AND DISCUSSIONS

Firstly, we describe the effects of a Mn impurity without any compensating oxygen vacancy (Mn_{Ti}). The charge density $\rho(r)$ is computed using spin-polarized DFT, DFT+U, and DFT+DMFT (Fig. 1). The difference in $\rho(r)$ in DFT and DFT+U shows that DFT places more charge on the Mn atoms compared to DFT+U (Fig1b). DFT+DMFT always places more charge on the Mn atom than other two methods.

To better understand these differences, we compare the total and the partial densities of states (DOS) for spin-polarized DFT, DFT+U, and DFT+DMFT (Fig. 2). The partial DOS shows that most of the contribution around E_F is from O-atoms (Fig. 2a-c). The 3d-occupation is consistent with Mn^{4+} in both DFT and DFT+U, as found in previous DFT-based studies^{18,31} (Table I). Although the non-magnetic DFT predicts the occupation to be 4.65, it puts the Mn d orbital at E_F , and results a metallic solution³¹. The magnetic moment in DFT+U is $2.67 \mu_B$ inside the Mn muffin-tin sphere for Mn atom and $0.24 \mu_B$ for the interstitial, giving a total moment of $2.91 \mu_B$. The total moment of the entire cell is $3.0 \mu_B$ (Table I). The equal magnetic moment in DFT and DFT+U can also be noticed from the integration of the spin-density (Fig. 2d) of the d orbital until E_F .

The computed Mn 3d occupation in DFT+DMFT is 4.44, and the average fluctuating local moment is $3.08 \mu_B$.

Method	System	Magnetic Moment (μ_B)	Occupation	Band Gap (eV)
NM-DFT	Mn_{Ti}	—	4.65	0.00
SP-DFT	Mn_{Ti}	3.00	3.16(up), 0.87(dn)	1.46
DFT+U	Mn_{Ti}	3.00	3.42(up), 1.07 (dn)	1.70
DFT+DMFT	Mn_{Ti}	3.08	4.44	1.14
NM-DFT	Mn_{Ti}VO	—	4.79	0.00
SP-DFT	Mn_{Ti}VO	4.47	3.78(up), 0.51 (dn)	0.00
DFT+U	Mn_{Ti}VO	5.00	3.34(up), 0.34 (dn)	1.15
DFT+DMFT	Mn_{Ti}VO	4.16	4.80	1.80

TABLE I. Computed magnetic moment (in μ_B), occupation of Mn d -orbital, and band gap(eV) for Mn in BaTiO_3 with and without O-vacancy obtained within non-magnetic (NM) DFT, spin-polarized(SP) DFT with ferromagnetic order, DFT+U and DFT+DMFT methods. Here DFT+DMFT is performed in paramagnetic phase of the materials and the magnetic moments in DFT+DMFT represent the average fluctuating local moment; the occupations in DFT and DFT+U are obtained by integrating the projected DOS to the Fermi energy.

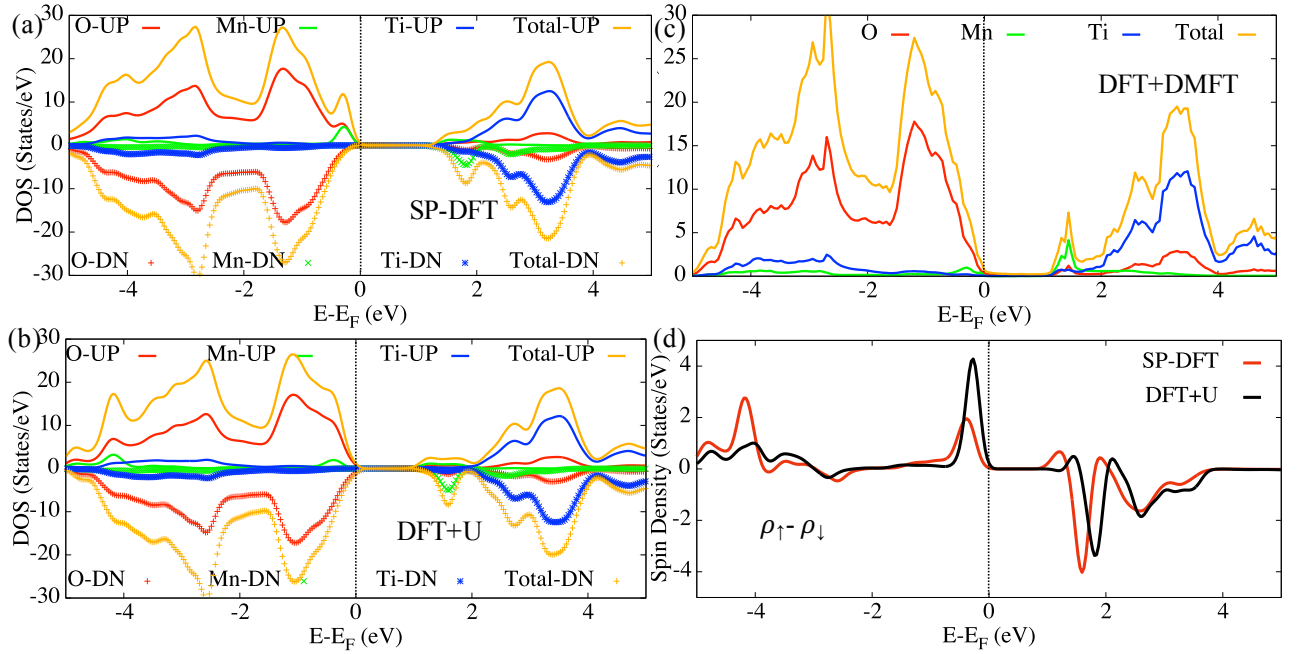


FIG. 2. (Color online). Spin decomposed total and projected densities of states (DOS) computed in (a) DFT, (b) DFT+U, and (c) DFT+DMFT methods for Mn substitution of Ti in BaTiO_3 without any compensating oxygen vacancy (Mn_{Ti}); (d) Computed spin density ($\rho_{\uparrow} - \rho_{\downarrow}$) with DFT and DFT+U (d) for the same system.

We compare our results with different double counting (DC) schemes; a fully localized limit form of double counting or FLL as introduced in Ref.⁴⁷, “nominal” DC as introduced in^{52,53} and “exact” double counting⁴⁸. We use both density-density form of the Coulomb repulsion (Ising) and the full Coulomb repulsion (Full) in rotationally invariant Slater form (Table II)⁵⁴. Changing U does not affect the d -occupation significantly. Keeping $J_H=0.8$ eV and varying U from 2 eV to 6 eV, the occupation changes from 4.74 to 4.78. Also keeping U fixed at 6 eV and varying J_H from 0 to 1.2 eV, the occupation changes from 4.30 and 4.40 and reaches its maximum value of 4.77 for $J_H=0.8$ eV.

We next discuss the results for Mn doped BTO with

a compensating oxygen vacancy along the z -direction (Mn_{Ti}VO)¹⁸. Interestingly, the computed occupancy of $\text{Mn}_{Ti}\text{-VO}$ is found to be $3d^5$ in either DFT, DFT+U, or DFT+DMFT (Table I). For DFT and DFT+U, we find the moment to be 4.47 and 5.00 μ_B respectively for the entire cell. In DFT+U, the Mn muffin-tin sphere has 4.28 μ_B and interstitial has 0.51 μ_B , giving a total of 4.79 μ_B . In the case of SP-DFT we find a metallic solution, where the Mn muffin-tin sphere has 3.6 μ_B and interstitial has 0.51 μ_B , giving a total of 4.11 μ_B .

We now discuss the valence fluctuations of Mn in DFT+DMFT, where the ground-state wave function is not restricted to being a single multiplet, as in DFT+U. On a single atom, there are 1024 different possible multi-

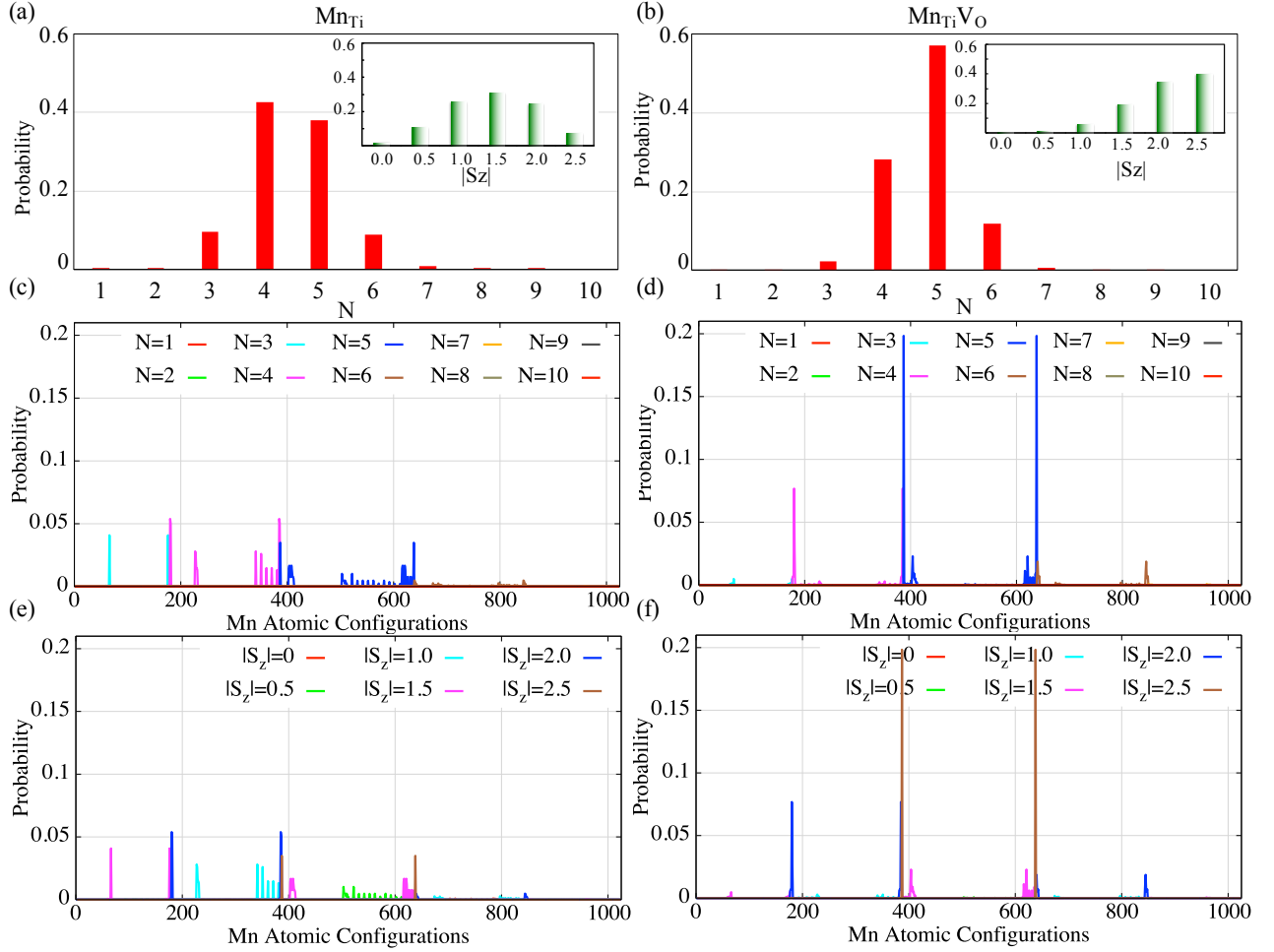


FIG. 3. (Color online). DFT+DMFT computed atomic histogram of the Mn $3d$ shell for Mn substituted BaTiO_3 (left) without (Mn_{Ti}) and (right) with (Mn_{TiVO}) compensating oxygen vacancy: (a -b) decomposed in number of particles N and (inset) spin-state (S_z); probability distribution for all 2^{10} ($=1024$) atomic configurations sorted for each N (c-d) and for each spin-state (e-f); N and S_z values are denoted with various colors.

DC	Coulomb	n_d
Exact	Ising	4.44
Exact	Full	4.39
Nominal	Ising	4.75
FLL	Full	4.76
FLL	Ising	4.77

TABLE II. DFT+DMFT computed occupation of d -orbital in Mn_{Ti} using different double counting and Coulomb schemes^{47,48,52,53,55}.

plets for d -electrons, characterized by different valences, orbital occupations, and spins³⁵. The histograms in Fig. 3 describe the probability of finding a Mn atom in the solid in each multiplets, and show that any method that considers only a single multiplet, such as even single determinant group state Quantum Monte Carlo will only be approximate. We find many occupied multiplets, such as $3d^3$, $3d^4$ and $3d^5$ with a maximum occupation of

$3d^4$ for Mn_{Ti} and $3d^5$ for Mn_{TiVO} (Fig. 3a-b). Without compensation, we find only about 5% weight in the most probable configurations. With a compensating vacancy, the fluctuations are smaller, but still there is only about 20% weight in the most likely multiplets. In Mn_{Ti} the sum of the probabilities are found to be 0.43, 0.34, 0.09 respectively for $N=4, 5$, and 6 . Thus the system is in a mixed valence state with an average d occupation of ~ 4.4 . For Mn_{TiVO} , the sum of the probabilities are 0.28, 0.57, 0.11 for $N=4, 5$, and 6 respectively. The difference in probabilities between $N=4$ and $N=5$ reduces with compensating oxygen vacancy in Mn_{TiVO} (Fig. 3b); the probability for $N=5$ increases and becomes the most probable state. This leads to an increase in average $3d$ occupation from 4.4 to 4.8 with compensating O-vacancy.

The histograms of the CTQMC (Inset of Fig. 3a-b) show the largest probability for the spin state $S_z=1.5$ for Mn_{Ti} and $S_z=2.5$ for Mn_{TiVO} . The histograms also show strong spin fluctuations. To identify the associated

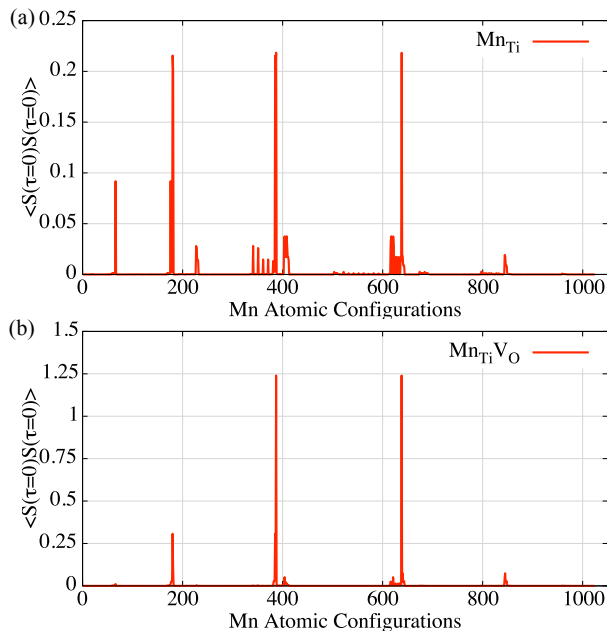


FIG. 4. (Color online) DFT+DMFT computed squared fluctuating local moment or the averaged spin-spin correlation function (a) for Mn substituted BaTiO₃ without (Mn_{Ti}) and (b) with compensating oxygen vacancy (Mn_{Ti}VO).

spin state for each eigenstate, we present them in various colors in Fig. 3(e-f). Here the first (last) few states with a particular N show the high (low) spin state (Fig. 3c-f). For Mn_{Ti}, we clearly see the spikes in probability for the high spin states ($S_z = 2, 2.5$) at the beginning of the constant N interval as well as for the low spin states ($S_z = 0, 0.5$), at the end of the constant N interval (Fig. 3c and 3e). For Mn_{Ti}VO we see spikes in probability for high spin states ($S_z = 2, 2.5$) are dominated than that for the low spin states ($S_z = 0, 0.5$) (Fig. 3d and 3f) for N=4 and N=5. The overall probability distribution changes significantly with oxygen vacancy and peaks mainly for N=5 and $S_z = 2.5$. Thus both the charge and spin fluctuations are reduced in Mn_{Ti}VO since the hopping of the electrons from Mn to neighboring oxygen is reduced due to the compensating vacancy. The dominance of the $S_z = 2.5$ configuration implies that Mn in BTO has a predominantly high spin state in Mn_{Ti}VO. The increase in magnetic moment with O-vacancy, as found in Table I, can be explained from the DFT+DMFT computed time averaged spin-spin correlation function ($\langle S(\tau=0)S(\tau=0) \rangle$) or the squared fluctuating local moment (Fig. 4), where we find an increase in the local moment in Mn_{Ti}VO. Reduced fluctuation and increased probability for electron to spend more time in the high spin states with O-vacancy gives rise to the increase in average fluctuating

local moment.

IV. CONCLUSIONS

Unlike previous density functional based studies yielding either high (Mn^{2+}) or low spin (Mn^{4+}) state of Mn in BaMn_{1-x}Ti_xO₃ with and without compensating oxygen vacancy respectively, DFT+DMFT predicts a mixed valence state of Mn in either system. Without compensating oxygen vacancies, the ground state in DFT+DMFT is found to be a quantum superposition of two distinct atomic valences, $3d^4$ and $3d^5$. Introducing a compensating oxygen vacancy at a neighboring site of Mn reduces hopping of electron from Mn to its ligand. This results in reduction of both charge and spin fluctuations. We conclude that the charge and valence fluctuations in 3d-transition metal doped BTO are strong, and are not captured by conventional DFT or DFT+U. DFT+DMFT predicted average valence of Mn in BTO is $3d^{2+}$ and $3d^{3.5+}$ with and without compensating oxygen vacancy respectively. The most important result presented here are the extreme fluctuations predicted, with only a small fraction in any given multiplet, and very different from DFT+U which assumes a single multiplet to be occupied. Even very accurate methods such as diffusion Monte Carlo generally consider only a single Slater determinant for solids. DFT+DMFT gives a new insight into the fluctuating states in correlated solids, which is presently challenging to represent by other standard methods. Our predictions of valence fluctuations in transition metal doped ferroelectrics can be verified, as was done in heavy Fermion system through hard X-ray photoemission study⁵⁶, in topological Kondo insulators through muon spin relaxation studies^{57,58} and in perovskite through Mossbauer spectroscopy⁵⁹ and NMR⁶⁰.

V. ACKNOWLEDGEMENT

This research was supported by the office of Naval Research (ONR) grants N00014-12-1-1038 and N00014-14-1-0561 and by the Carnegie Institution of Washington. S. M acknowledges the support from the NSF SI2-SSI program (Grant No. ACI-1339804). K. H acknowledges the supports from NSF DMR-1405303. REC is supported by the Carnegie Institution and by the European Research Council advanced grant ToMCaT. Computations were performed at the ‘Supermike’ at the Louisiana State University and NERSC supercomputing facility. We thank Sohrab Ismail-Beigi, Ivan I. Naumov and Javier F. Nossas for helpful discussions to prepare this manuscript. We acknowledge Peng Zhang, Mark Jarrell and Juana Moreno for their important help.

¹ D. V. Efremov, J. van den Brink, and D. I. Khomskii, Nat. Mater **3**, 853 (2004).

² C. Ederer and N. A. Spaldin, Nat. Mater **3**, 849 (2004).

- ³ D. P. Norton, N. A. Theodoropoulou, A. F. Hebard, J. D. Budai, L. A. Boatner, S. J. Pearton, and R. G. Wilson, *Electrochemical and Solid-State Letters*, **6**, G19 (2003).
- ⁴ H. K. Chandra, K. Gupta, A. K. Nandy, and P. Mahadevan, *Phys. Rev. B* **87**, 214110 (2013).
- ⁵ Y. Shuai, S. Zhou, D. Brger, H. Reuther, I. Skorupa, V. John, M. Helm, and H. Schmidt, *J. Appl. Phys.* **109**, 084105 (2011).
- ⁶ X. Tong, Y.-H. Lin, S. Zhang, Y. Wang, and C.-W. Nan, *Journal of Applied Physics* **104**, 066108 (2008).
- ⁷ R. Bottcher, H. T. Langhammer, T. Muller, and H.-P. Abicht, *J. Phys.: Condens. Matt.* **17**, 4925 (2005).
- ⁸ O. D. Jayakumar, H. G. Salunke, R. M. Kadam, M. Mohapatra, G. Yaswant, and S. K. Kulshreshtha, *Nanotechnology* **17**, 1278 (2006).
- ⁹ R. Bottcher, H. T. Langhammer, T. Muller, and H.-P. Abicht, *J. Phys. Cond. Matt.* **20**, 505209 (2008).
- ¹⁰ H. T. Langhammer, T. Muller, R. Bttcher, and H.-P. Abicht, *J. Phys. Cond. Matt.* **20**, 085206 (2008).
- ¹¹ X.-X. Wu, W. Fang, W.-L. Feng, and W.-C. Zheng, *Pramana* **72**, 569 (2009).
- ¹² N. V. Dang, T. D. Thanh, L. V. Hong, V. D. Lam, and T.-L. Phan, *Journal of Applied Physics* **110**, 043914 (2011).
- ¹³ N. V. Dang, T.-L. Phan, T. D. Thanh, V. D. Lam, and L. V. Hong, *Journal of Applied Physics* **111**, 113913 (2012).
- ¹⁴ T.-L. Phan, P. Zhang, D. Grinting, S. C. Yu, N. X. Nghia, N. V. Dang, and V. D. Lam, *Journal of Applied Physics* **112**, 013909 (2012).
- ¹⁵ S. K. Gupta, R. Kadam, R. Gupta, M. Sahu, and V. Natarajan, *Mat. Chem. Phys.* **145**, 162 (2014).
- ¹⁶ X. Ren, *Nature Materials* **3**, 91 (2004).
- ¹⁷ L. X. Zhang and X. Ren, *Physical Review B* **71** (2005).
- ¹⁸ J. F. Nossia, I. I. Naumov, and R. E. Cohen, *Phys. Rev. B* **91**, 214105 (2015).
- ¹⁹ J. B. J. Chapman, R. E. Cohen, A. V. Kimmel, and D. M. Duffy, *Phys Rev Lett* **119**, 177602 (2017).
- ²⁰ S. Liu and R. E. Cohen, *Applied Physics Letters* **111**, 082903 (2017).
- ²¹ T. Dietl, *Nat Mater* **9**, 965 (2010).
- ²² K. Sato, L. Bergqvist, J. Kudrnovsk, P. H. Dedrichs, O. Eriksson, I. Turek, B. Sanyal, G. Bouzerar, H. Katayama-Yoshida, V. A. Dinh, T. Fukushima, H. Kizaki, and R. Zeller, *Reviews of Modern Physics* **82**, 1633 (2010).
- ²³ L. Pauling, *The nature of the chemical bond*, 3rd ed. (Cornell University Press, 1960).
- ²⁴ Y. Quan, V. Pardo, and W. E. Pickett, *Phys. Rev. Lett.* **109**, 216401 (2012).
- ²⁵ L. Jiang, S. V. Levchenko, and A. M. Rappe, *Phys. Rev. Lett.* **108**, 166403 (2012).
- ²⁶ P. H.-L. Sit, R. Car, M. H. Cohen, and A. Selloni, *Inorganic Chemistry* **50**, 10259 (2011).
- ²⁷ W. E. Pickett, Y. Quan, and V. Pardo, *Journal of Physics: Condensed Matter* **26**, 274203 (2014).
- ²⁸ B. Cheng, B. F. Hu, R. Y. Chen, G. Xu, P. Zheng, J. L. Luo, and N. L. Wang, *Phys. Rev. B* **86**, 134503 (2012).
- ²⁹ A. B. Georgescu and S. Ismail-Beigi, *Phys. Rev. B* **96**, 165135 (2017).
- ³⁰ N. V. Dang, T. D. Thanh, L. V. Hong, V. D. Lam, and T.-L. Phan, *J. App. Phys.* **110**, 043914 (2011).
- ³¹ H. Nakayama and H. Katayama-Yoshida, *Jpn. J. Appl. Phys.* **40**, L1355 (2001).
- ³² G. Kotliar, S. Y. Savrasov, K. Haule, V. S. Oudovenko, O. Parcollet, and C. A. Marianetti, *Rev. Mod. Phys.* **78**, 865 (2006).
- ³³ J. H. Shim, K. Haule, and G. Kotliar, *Nature* **446**, 513 (2007).
- ³⁴ P. Zhang, R. E. Cohen, and K. Haule, *Nature* **517**, 605 (2015).
- ³⁵ Z. P. Yin, K. Haule, and G. Kotliar, *Nat. Mater.* **10**, 932 (2011).
- ³⁶ M. Liu, L. W. Harriger, H. Luo, M. Wang, R. A. Ewings, T. Guidi, H. Park, K. Haule, G. Kotliar, S. M. Hayden, and P. Dai, *Nat. Phys.* **8**, 376 (2012).
- ³⁷ M. Wang, C. Zhang, X. Lu, G. Tan, H. Luo, Y. Song, M. Wang, X. Zhang, E. A. Goremychkin, T. G. Perring, T. A. Maier, Z. Yin, K. Haule, G. Kotliar, and P. Dai, *Nat. Comm.* **4**, 1 (2013).
- ³⁸ S. J. Schafgans, A. A. and Moon, B. C. Pursley, A. D. LaForge, M. M. Qazilbash, A. S. Sefat, D. Mandrus, K. Haule, G. Kotliar, and D. N. Basov, *Phys. Rev. Lett.* **108**, 147002 (2012).
- ³⁹ S. Mandal, R. E. Cohen, and K. Haule, *Phys. Rev. B* **89**, 220502(R) (2014).
- ⁴⁰ S. Mandal, R. E. Cohen, and K. Haule, *Phys. Rev. B* **90**, 060501(R) (2014).
- ⁴¹ S. Mandal, P. Zhang, S. Ismail-Beigi, and K. Haule, *Phys. Rev. Lett.* **119**, 067004 (2017).
- ⁴² J. Kunes, A. V. Lukoyanov, V. I. Anisimov, R. T. Scalettar, and W. E. Pickett, *Nat. Mater* **7**, 198 (2008).
- ⁴³ K. Haule, C.-H. Yee, and K. Kim, *Phys. Rev. B* **81**, 195107 (2010).
- ⁴⁴ P. Blaha, K. Schwarz, G. Madsen, D. Kvasnicka, and J. Luitz, *An augmented plane wave plus local orbitals program for calculating crystal properties*, edited by K. Schwarz (Vienna University of Technology, Austria, 2001, 2001).
- ⁴⁵ Z. Wu and R. E. Cohen, *Phys. Rev. B* **73**, 235116 (2006).
- ⁴⁶ A. Kutepov, K. Haule, S. Y. Savrasov, and G. Kotliar, *Phys. Rev. B* **82**, 045105 (2010).
- ⁴⁷ M. T. Czyżyk and G. A. Sawatzky, *Phys. Rev. B* **49**, 14211 (1994).
- ⁴⁸ K. Haule, *Phys. Rev. Lett.* **115**, 196403 (2015).
- ⁴⁹ Rutgers DFT+DMFT software: <http://hauleweb.rutgers.edu/tutorials>.
- ⁵⁰ X. Gonze, B. Amadon, P.-M. Anglade, J.-M. Beuken, F. Bottin, P. Boulanger, F. Bruneval, D. Caliste, R. Caracas, M. Ct, T. Deutsch, L. Genovese, P. Ghosez, M. Giantomassi, S. Goedecker, D. Hamann, P. Hermet, F. Jollet, G. Jomard, S. Leroux, M. Mancini, S. Mazevet, M. Oliveira, G. Onida, Y. Pouillon, T. Rangel, G.-M. Rignanese, D. Sangalli, R. Shaltaf, M. Torrent, M. Verstraete, G. Zerah, and J. Zwanziger, *Computer Physics Communications* **180**, 2582 (2009), 40 YEARS OF CPC: A celebratory issue focused on quality software for high performance, grid and novel computing architectures.
- ⁵¹ X. Gonze, G. Rignanese, M. Verstraete, J. Betiken, Y. Pouillon, R. Caracas, F. Jollet, M. Torrent, G. Zerah, M. Mikami, P. Ghosez, M. Veithen, J.-Y. Raty, V. Olevano, F. Bruneval, L. Reining, R. Godby, G. Onida, D. Hamann, and D. Allan, *Zeitschrift für Kristallographie*. (Special issue on Computational Crystallography) **220**, 558 (2005).
- ⁵² K. Haule, C.-H. Yee, and K. Kim, *Phys. Rev. B* **81**, 195107 (2010).
- ⁵³ K. Haule, T. Birol, and G. Kotliar, *Phys. Rev. B* **90**, 075136 (2014).

- ⁵⁴ [Http://hauleweb.rutgers.edu/tutorials/CoulombUexplain.html](http://hauleweb.rutgers.edu/tutorials/CoulombUexplain.html).
- ⁵⁵ A. Georges, L. de' Medici, and J. Mravlje, *Annual Review of Condensed Matter Physics* **4**, 137 (2013).
- ⁵⁶ M. Okawa, M. Matsunami, K. Ishizaka, R. Eguchi, M. Taguchi, A. Chainani, Y. Takata, M. Yabashi, K. Tamasaku, Y. Nishino, T. Ishikawa, K. Kuga, N. Horie, S. Nakatsuji, and S. Shin, *Phys. Rev. Lett.* **104**, 247201 (2010).
- ⁵⁷ P. K. Biswas, Z. Salman, T. Neupert, E. Morenzoni, E. Pomjakushina, F. von Rohr, K. Conder, G. Balakrishnan, M. C. Hatnean, M. R. Lees, D. M. Paul, A. Schilling, C. Baines, H. Luetkens, R. Khasanov, and A. Amato, *Phys. Rev. B* **89**, 161107 (2014).
- ⁵⁸ K. Akintola, A. Pal, M. Potma, S. R. Saha, X. F. Wang, J. Paglione, and J. E. Sonier, *Phys. Rev. B* **95**, 245107 (2017).
- ⁵⁹ J. Linden, T. Yamamoto, M. Karppinen, H. Yamauchi, and T. Pietari, *Applied Physics Letters* **76**, 2925 (2000).
- ⁶⁰ J. Zhang, L. Ma, J. Dai, Y. P. Zhang, Z. He, B. Normand, and W. Yu, *Phys. Rev. B* **89**, 174412 (2014).